Aging of high power Li-ion cells during real use of electric vehicles

Nassim Rizoug, Redha Sadoun, Tedjani Mesbahi, Patrick Bartholumeus, Philippe Lemoigne

▶ **To cite this version:**

Nassim Rizoug, Redha Sadoun, Tedjani Mesbahi, Patrick Bartholumeus, Philippe Lemoigne. Aging of high power Li-ion cells during real use of electric vehicles. IET Electrical Systems in Transportation, 2017, 7 (1), pp.14-22. 10.1049/iet-est.2016.0012 . hal-04549353

HAL Id: hal-04549353
https://hal.science/hal-04549353

Submitted on 17 Apr 2024

HAL is a multi-disciplinary open access archive for the deposit and dissemination of scientific research documents, whether they are published or not. The documents may come from teaching and research institutions in France or abroad, or from public or private research centers.

L'archive ouverte pluridisciplinaire **HAL**, est destinée au dépôt et à la diffusion de documents scientifiques de niveau recherche, publiés ou non, émanant des établissements d'enseignement et de recherche français ou étrangers, des laboratoires publics ou privés.

Distributed under a Creative Commons Attribution 4.0 International License

IET Electrical Systems in Transportation

Special Issue: Design, Modeling and Control of Electric Vehicles: Selected Papers from IEEE Vehicle Power and Propulsion Conference (VPPC 2015)

Aging of high power Li-ion cells during real use of electric vehicles

ISSN 2042-9738
Received on 23rd February 2016
Revised 23rd December 2016
Accepted on 6th January 2017
E-First on 14th March 2017
doi: 10.1049/iet-est.2016.0012
www.ietdl.org

Nassim Rizoug[1] ✉, Redha Sadoun[2], Tedjani Mesbahi[3], Patrick Bartholumeus[3], Philippe LeMoigne[3]

[1]S2ET-Ecole Supérieure des Techniques Aéronautiques et de Construction Automobile, Rue Georges Charpak BP76121, 53061 LAVAL Cedex 9, France

[2]Assystem SA, 23 place de Wicklow 78180 Montigny le Bretonneux, France

[3]Univ. Lille, Centrale Lille, Arts et Metiers ParisTech, HEI, EA 2697 – L2EP – Laboratoire d'Electrotechnique et d'Electronique de Puissance, F-59000 Lille, France

✉ *E-mail: nassim.rizoug@estaca.fr*

Abstract: Currently, the vehicle manufacturers use the high power Li-ion technology to supply the electric and hybrid vehicles. This technology is able to ensure the power needed to propel the vehicle. Until now several studies have been made by the laboratories and manufacturers to characterise this technology. The aim of these test (electric, thermal, aging,…) is to make comparison between Li-ion technologies and choice the best one for each application. For that, they use accelerated cycling with different condition to characterise cells, what can reduce the tests duration. Unfortunately, this type of cycle cannot give us information about the aging of HP Li-ion technology under real use of the vehicle. Firstly, the requirements specification (vehicle specification, battery technologies, mission) has been presented. After that, the authors will present the test bench developed in the laboratory to characterise batteries and study the aging of the HP technology. Here the authors present the study of the Li-ion HP behaviour during almost 3 years and the modelling (electric, thermal and aging modelling) using a real driving cycle. The experimental results are compared with the results obtained with the developed ageing model. The obtained results prove the good performances of this technology in electric vehicle applications.

1 Introduction

The energy challenge pushes the industrial world and especially the vehicles manufacturers to look for green solutions. One of the current solutions is the use of electric energy as an alternative to reduce the release of greenhouse gases. Unfortunately, the used sources for this type of vehicle do not perfectly conform to the specifications in terms of range, available power and durability. In this context, electrochemistry researchers have doubled the effort to improve the characteristics of Li-ion technology by strengthening the design of this technology. High power (HP) Li-ion technology is one of these developed technologies, which provide adapted performances for electric vehicles with a very high specific power to ensure acceleration and energy recovery during braking. The behaviour of this technology has been the subject of several works of literature. To reduce the study duration, these works use the accelerated cycling to compare the performance of this technology to other existing technologies. For that, we cannot use these results to obtain the behaviour of this technology in real use of the vehicle. In this paper, we are interested by the study of the Li-ion HP cells behaviour with real driving cycle, which includes an urban part and a suburban part. We started with the modelling of electrical behaviour before studying the thermal behaviour of these technologies ending with aging model of the cells. The processing of data saved during 3 years of cycling, allows us to study the degradation of this technology during 472,500 km of vehicle use.

2 Sizing and management requirements

2.1 Cycle and mission

The assessment and reliability of transport emission models inventory systems (ARTEMIS driving cycle) is the chosen profile in our study. This mission is based on analysis of data from previous work such as research projects MODEM-HyZEM and driving cycles for light vehicles (INRETS-PVU) [1]. Three cycles (urban, road and motorway) have been carried out to describe the sequence and reproduce the real conditions of the vehicle use. In our case, the test cycle consists of both urban and road driving profiles, as shown in Fig. 1. The urban part has an average speed of about 7.5 km/h. However, the average speed of the road driving part is 61.3 km/h with a top speed of 110.7 km/h. The combination of urban and road profiles can simulate a rolling distance of 22 km over a period of about 34 min [2]. The ARTEMIS cycle has much closer driving dynamics of the reality. That is why we have selected for this study.

2.2 Vehicle characteristics

The electric vehicle (EV) power and energy consumptions dependent on the driving cycle and the characteristics of the vehicle in terms of weight, volume, air drag coefficient (Cx)…etc. Our work is based on the study of consumption of an urban type of EV, the parameters are given in Table 1. It must be noted that the weight (WEV) entered in this table, represents the weight of all the EV components (chassis, interior…) but does not include the weight of the energy storage system (ESS). The influence of the ESS weight will be integrated to enable solvency problem without an iterative process. Indeed, the proportion of the ESS weight in EV is not negligible.

2.3 Battery technologies

Currently, the regular EV is supplied by a battery pack. This pack is made up of modules connected in series and/or parallel depending on the supply voltage and the desired storage capacity. Each module is composed of a number of battery cells. The connecting devices and protection are an additional weight and volume in the battery pack. A study of existing battery packs on the market has allowed us to evaluate the weight and volume of these devices. We can consider that the weight and the additional volume can be estimated at about 40% of the weight and volume of cells.

© The Institution of Engineering and Technology 2017

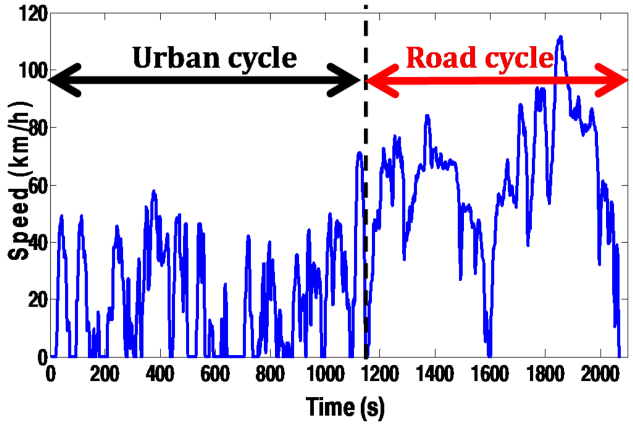

Fig. 1 *ARTEMIS driving cycle*

This assumption is valid also for other ESSs such as supercapacitors.

Table 2 gives the characteristics of Li-ion battery cells considered for this study, which presents their most relevant specifications that can be found in its datasheet. To study the influence of performance of a cell sizing, we have selected some batteries HP density and others to high energy density (HE), marketed by both manufacturers DowKokam and Saft. The special feature of HP batteries is that they can withstand currents charging and discharging much more important than HE batteries. This characteristic represents one of the basic criteria for the design of batteries.

On the other hand, the specific energy of HE cells is higher than that of HP cells. In the same type of Li-ion battery (HP or HE) there are also disparities due to the chemical composition of the positive electrode [6].

3 Power and energy computation

The battery sizing power and energy are imposed by the EV dynamics using the speed cycle and slope profile. The needed power at the wheels P_V is expressed by:

$$P_V = C_T \cdot \Omega_{wheels} \tag{1}$$

Table 1 Car characteristics: Bluecar [3]

Parameter	Value
C_0: rolling coefficient	0.008
C_1: rolling cure coefficient	1.6E^{-6} s^2/m^2
C_x: aerodynamic drag coefficient	0.3
S: frontal area	2.75 m^2
WEV: weight of the EV without ESS (kg)	860 kg
R: wheel diameter	0.33 m

When the total torque C_T and wheels angular velocity Ω_{wheels} are calculated from the traction force F_T and the vehicle speed V_{VEH}:

$$\begin{cases} C_T = F_T \cdot r \\ \Omega_{wheels} = V_{VEH} \cdot r^{-1} \end{cases} \tag{2}$$

With r is the wheel radius.

The required force to propel the EV is given by the sum of the resistant forces and acceleration force Facc. As shown in Fig. 2*a*, resistant forces are detailed by the 3:

where F_{aero}: aerodynamic drag force. F_{roll}: the rolling resistance force. F_{gx}: gravitational force.

$$\begin{cases} F_{aero} = 0.5 \cdot \rho \cdot s \cdot C_x \cdot V_{VEH}^2 \\ F_{roll} = (M_{EV} + M_{ESS}) \cdot g \cdot (C_0 + C_1 \cdot V_{VEH}^2) \\ F_{gx} = (M_{EV} + M_{ESS}) \cdot g \cdot \sin(\propto) \end{cases} \tag{3}$$

These forces are expressed according to the EV and ESS weight (M_{EV} and M_{SSE}). As a result, the EV required power can be described as follows:

$$P_V = \left((M_{EV} + M_{ESS}) \cdot \frac{dV_{VEH}}{dt} + F_{aero} + F_{roll} + F_{gx} \right) \cdot V_{VEH} \tag{4}$$

Fig. 2*b* shows the power and energy required for propulsion of EV using ARTEMIS driving cycle. The positive power is the power that the propulsion system transmits to the wheels. P_{V_cons} being the maximum value of the consumed power. The negative portion represents the power recovered during braking phases and P_{V_rec} is the maximum value of recovered power. The energy consumed is obtained by integration of the vehicle power during the entire mission (tcy). The E_{V_cons} parameter is the energy necessary to achieve the needed range of EVs. The driving cycle is repeated as necessary to achieve the desired range. For instance, in Fig. 2*b*, the ARTEMIS cycle is repeated 7 times to achieve 150 km of driving range (22 kmX7≃150 km):

$$E_{V\_cons} = \int_0^{t_{cy}} P_V(t) \cdot dt \tag{5}$$

The P_{V_cons}. P_{V_rec} powers and E_{V_cons} energy are the main constraints which influence the ESS sizing. These parameters depend on the velocity profile, the roadway slope, and the desired driving range.

4 Sizing of the storage system

The constraints provided by the vehicle dynamic are the maximum power consumption and the energy needed to achieve the required range. In this case, is not necessarily to recover the totally of the

Table 2 Specifications of used Li-ion cells, [4, 5]

	HP Li-ion Cells			HE Li-ion Cells		
Acronyme	Ko40HP	Ko100HP	Sa34HP	Ko40HE	Ko100HE	Sa45HE
costumer	DowKokam	DowKokam	Saft	DowKokam	DowKokam	Saft
electrodes chemistry(E. negative/E. positive)	Graphite/ LiMnNiCo02	Graphite/ LiMnNiCo02	Graphite/ LiMnNiCo02	Graphite/ LiMnNiCo02	Graphite/ LiMnNiCc02	Graphite/ LiFePO4
nominal voltage, V	3.70	3.70	3.65	3.70	3.70	3.30
nominal Capacity, Ah	40.00	100.00	33.00	40.00	100.00	44.00
interne resistance, mΩ	0.80	0.55	1.00	0.90	0.65	1.20
charge/discharge rates, A	80/200	200/500	120/500	40/40	100/100	6.28/50
specific energy, Wh/kg	143.68	148.00	128.00	167.25	164.44	155.55
weight, kg	1.030	2.500	0.940	0.885	2.250	0.90
volume, l	0.508	1.140	0.410	0.441	1.066	0.48
cost, €	82.22	209.90	67.80	76.33	190.81	72.24

© The Institution of Engineering and Technology 2017

20429746, 2017, 1, Downloaded from https://ietresearch.onlinelibrary.wiley.com/doi/10.1049/iet-est.2016.0012 by Cochrane France, Wiley Online Library on [17/04/2024]. See the Terms and Conditions (https://onlinelibrary.wiley.com/terms-and-conditions) on Wiley Online Library for rules of use; OA articles are governed by the applicable Creative Commons License

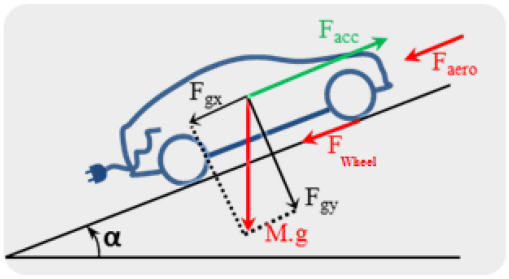

a

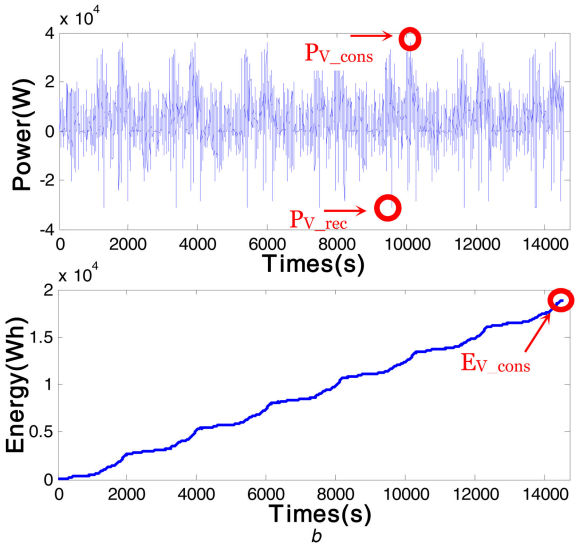

b

Fig. 2 *Forces, power and energy needed to propel the vehicle*
(a) Forces to propel the vehicle, ***(b)*** Power and energy profiles during 150 km

braking energy and a part of this last one must be dissipated in the mechanical braking system.

4.1 Batteries sizing algorithm

Based on the constraints ensured by the battery pack, we have developed the sizing algorithm, which is detailed in Fig. 3. The algorithm inputs are the characteristics of the battery cells and EV mission defined by the speed profile and the slope of the roadway. We distinguish generally in this algorithm two main steps:

- The first step is to compute the number of cells $N_{cells} = N_{S\_B} \cdot N_{P\_B}$ needed to ensure the maximum consumed power (P_{V_cons}).

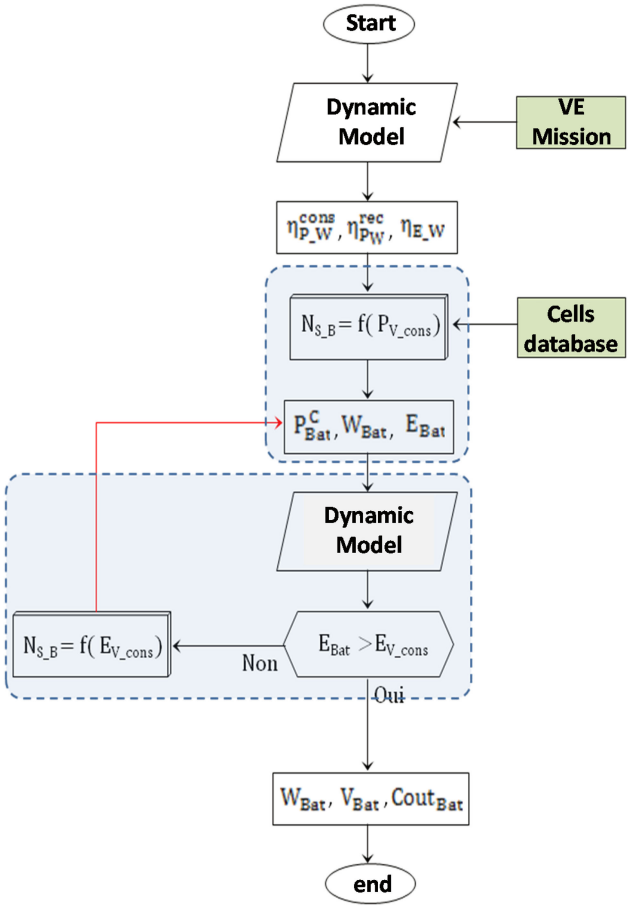

Fig. 3 *Flowchart of battery sizing algorithm*

This number of cells gives us the characteristic of the battery pack (power limits P^{C}_{Bat} and P^{Dis}_{Bat}, pack capacity, weight, volume. …)

Where N_{S_B} : number of cells in series. N_{P_B} : number of battery module in parallel.

- The limitation of battery charging power reduces the amount of energy recovered, in particular if the charging rate is low. Therefore, a second step is required to verify that the energy of this sized pack is sufficient to ensure the necessary driving range. If this is the case, the size characteristics (weight and volume) and cost of the ESS supplying the VE is given directly as a function of N_{cells} expressed according to the power consumed. Furthermore, if the energy is not sufficient, the battery pack is resized with respect to the energy consumed [7].

4.2 Sizing results

The sizing is carried out for the ARTEMIS driving cycle with a roadway slope of 2.5%. The velocity profile is repeated many times as necessary to achieve an EV driving range between 22–400 km [8].

Fig. 4*a* shows the batteries weight sized according to the desired driving range. We find that the results are evolving into two distinct groups: the group of HP batteries where the weight increases with the driving range and the group of HE batteries, where their weight is set to a constant for low driving range and becomes variable beyond 267 km of EV driving range. This is explained by the fact that for these batteries the energy available is largely sufficient to ensure the needed driving range. The most restrictive criterion is the power consumption and the value of this power is constant for both 22 and 44 km of driving range. For high-energy batteries, they are sized according to the needed power for lower and medium driving ranges. As shown in Fig. 4*a*, the Ko40HE batteries are sized according to the needed power until 267 km of driving range, and the maximum consumed power does not vary according to the needed driving range for the low ranges. Beyond 267 km, the requested driving range became more important and also set the criterion to compute the number of battery cells.

5 Test bench and simplification of the used cycle

To test the behaviour of storage systems in drivetrain applications, a test bench was developed in ESTACA'LAB laboratory. This bench is able to emulate the charge/discharge cycles under conditions similar to those used in real applications (electric power, energy storage, filtering, UPS … etc.). The developed test bench

© The Institution of Engineering and Technology 2017

20429746, 2017, 1, Downloaded from https://ietresearch.onlinelibrary.wiley.com/doi/10.1049/iet-est.2016.0012 by Cochrane France, Wiley Online Library on [17/04/2024]. See the Terms and Conditions (https://onlinelibrary.wiley.com/terms-and-conditions) on Wiley Online Library for rules of use; OA articles are governed by the applicable Creative Commons License

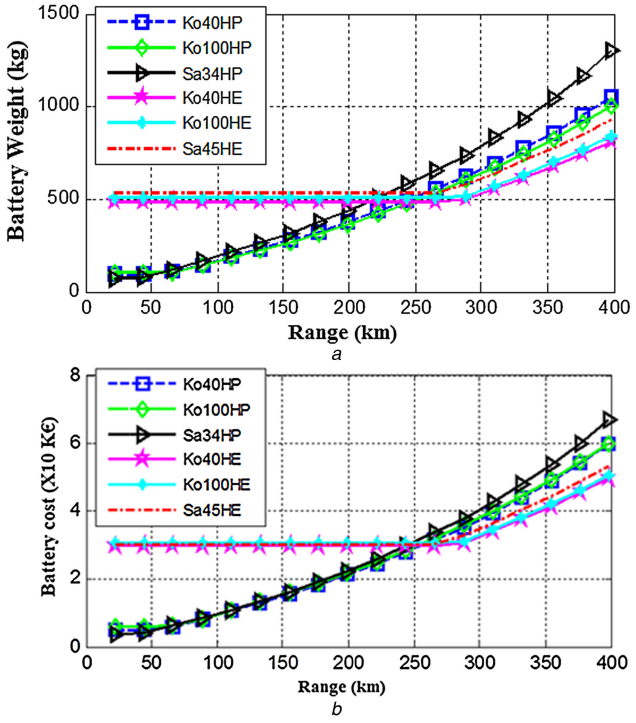

Fig. 4 *Batteries sized according to the needed driving range*
(a) Batteries weights, ***(b)*** Batteries cost

can track the behaviour of a system under electrical constraints 24 h/24 h [9].

Fig. 5*a* shows the diagram of the test bench. The cycling current is provided by the control of energy transit between the tested cells and buffer storage system. This last one is sized to store the energy of the tested cells during the discharge of these cells and restore this energy during the charging of these tested cells. For this, the capacity of the buffer unit is much larger than that of the tested cells. In our case, this capacity is 7 times higher than that of the tested cells. When the buffer unit is fully charged, the excess power is then dissipated in the resistive load of 9.6 kW. Finally, the energy dissipated during the cycling is compensated by a 10 kW power supply.

Fig. 6*a* shows a photograph of the bench (right-hand side). It is composed:

- Acquisition, control and supervision.
- Interface cards and four bridge converter 60 V/600 A).
- 10 kW power supply.
- Buffer module.

The tested cells are placed in a climatic chamber, which allows controlling the ambient temperature. This thermal conditioning keeps the outdoor temperature at 23°C in order to ensure the thermal homogeneity of tested cells.

As a regard of bench control, the CompactRIO Module, NI cRIO −9024, National Instruments was used to carry out both control of cycles and data acquisition with high accuracy. This module has a programmable FPGA with the LabVIEW environment. The embedded software can control the current

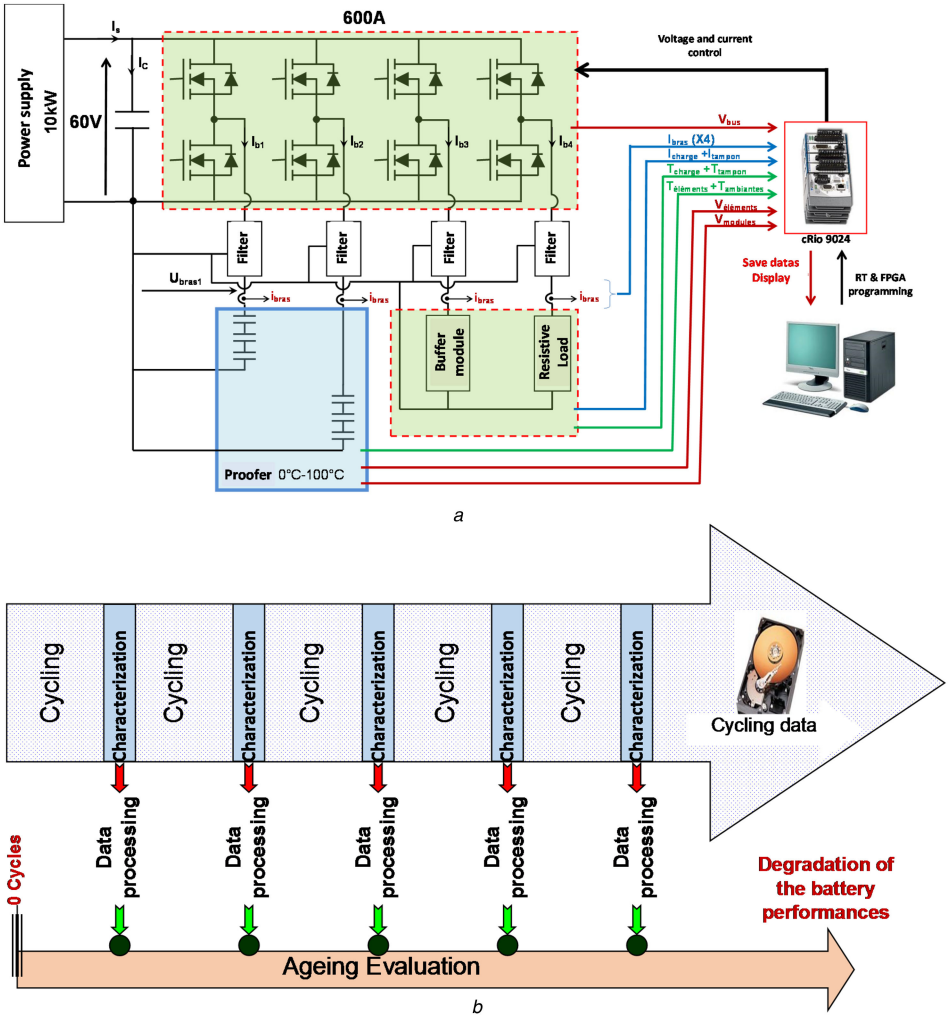

Fig. 5 *Using of the test bench to study the battery aging*
(a) Test bench synoptic (600 A, 60 V, 40 kHz), ***(b)*** Study of the battery aging

or/and the voltage of the tested cells. The deferent thermal, voltage

© The Institution of Engineering and Technology 2017

20429746, 2017, 1, Downloaded from https://ietresearch.onlinelibrary.wiley.com/doi/10.1049/iet-est.2016.0012 by Cochrane France, Wiley Online Library on [17/04/2024]. See the Terms and Conditions (https://onlinelibrary.wiley.com/terms-and-conditions) on Wiley Online Library for rules of use; OA articles are governed by the applicable Creative Commons License

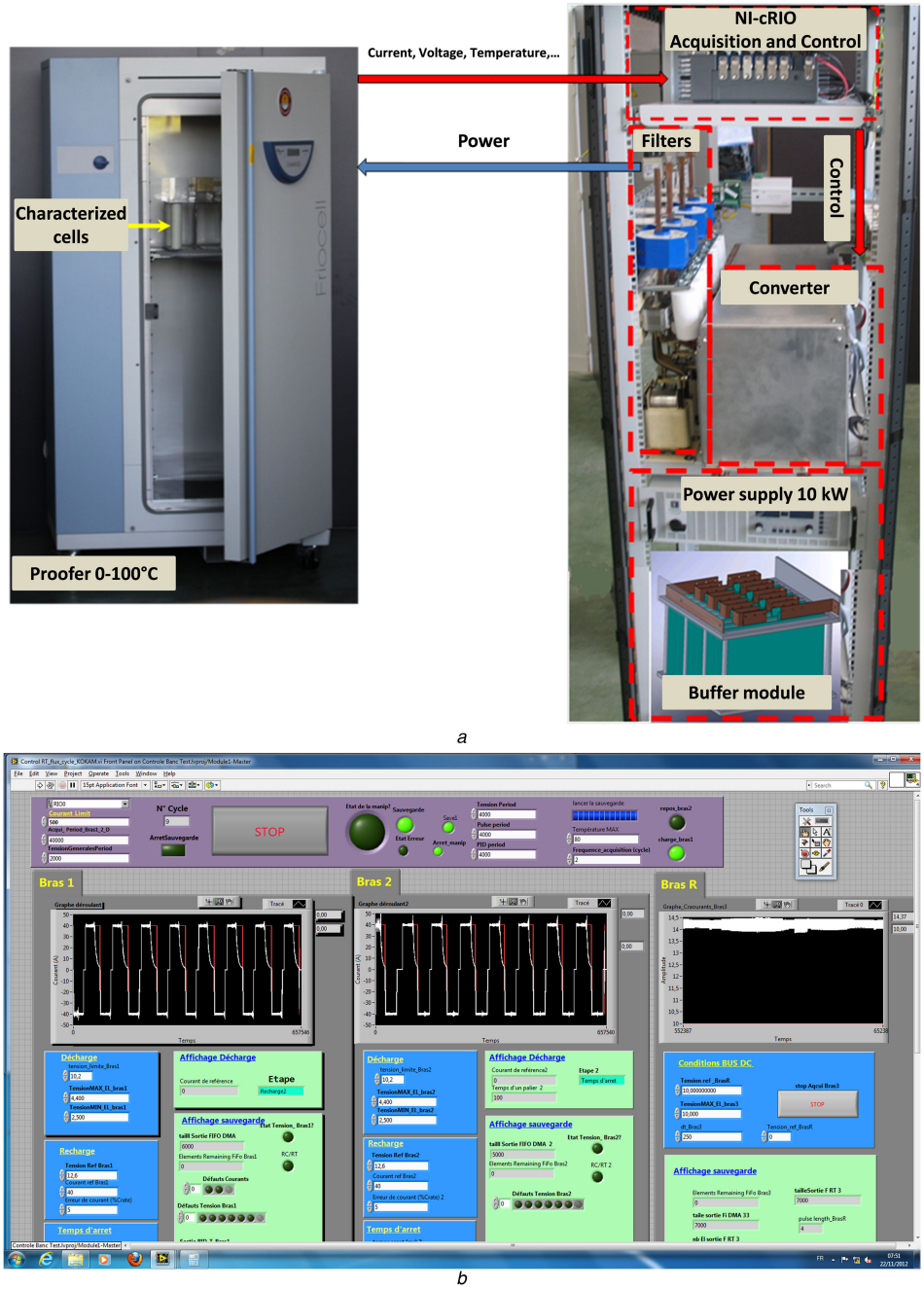

Fig. 6 *Test bench developed in ESTACA'Lab*
(a) Test bench photos, ***(b)*** HMI for the test bench steering

defaults are managed to stop the cycling and ensure the safety of the test bench. The control loops are programmed in LabVIEW FPGA and operate at a sampling frequency of 10 kHz.

The acquisition is also provided by the NI cRIO-9024 module. NI-9239 24bit resolution is used for the acquisition of cells voltages and currents. For the module voltages (voltage <60 V) NI-9229/24bit cards are used. The frequency acquisition of all electrical values is set at 1 kHz. For the acquisition of temperatures, the thermocouples are connected to NI9213 cards/ 24bits which have a lower sensitivity of 0.02°C. The temperature acquisition rate is fixed at 0.5 Hz.

5.1 Control and monitoring of the test bench

Fig. 6*b* presents the HMI interface of the real-time software. This last one allows the variation of the control and acquisition parameters, as well as managing the security of the bank (max and min voltage and current limits tolerated by the components. max limit of temperature…). This interface also allows us to view information about the status of the bench (defects, defect type, backup activation, the number of cycles performed….) and visualise the evolution of the electrical measures (voltages and currents) and cells temperatures.

5.2 Protocol of the aging study

The test procedure to evaluate the cycling impact on the battery cells is composed of two main phases:

- Cycling phase based on the real EV current profile.
- Characterisation phase which is measured during the variation of the internal resistance and capacity. (Fig. 5*b*).

5.3 Generation of the cycle profile

For this study, we have developed a method for the levels stress classification. The characteristic values that we considered with this approach are the current and the amount of exchanged charges.

Before applying this constraints classification, we have separated the urban and highway cycles and for each cycle, we

© The Institution of Engineering and Technology 2017

20429746, 2017, 1, Downloaded from https://ietresearch.onlinelibrary.wiley.com/doi/10.1049/iet-est.2016.0012 by Cochrane France, Wiley Online Library on [17/04/2024]. See the Terms and Conditions (https://onlinelibrary.wiley.com/terms-and-conditions) on Wiley Online Library for rules of use; OA articles are governed by the applicable Creative Commons License

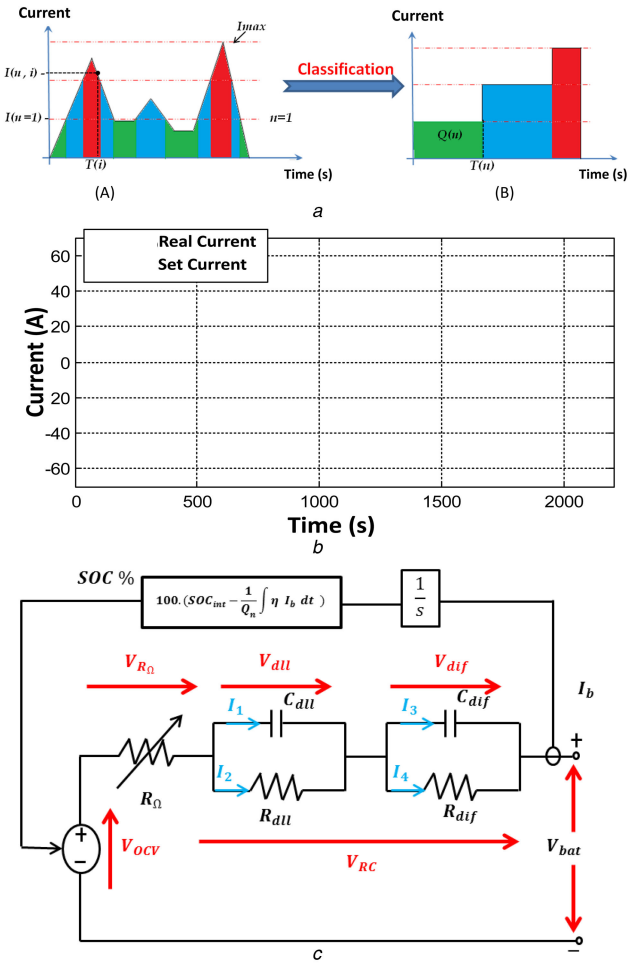

Fig. 7 *Battery cell equivalent model and cycle simplification*

(a) Simplified constraints (power, energy) applied to battery cells. (A) Real current. (B) Current after simplification and classification, ***(b)*** real and cycling currents, ***(c)*** Battery cell equivalent circuit model

decompose discharge phases and battery recharging. To explain the method, we use the simplified profile of Figs. 7*a* and *b*. Simplification steps are as follows:

- At the beginning, the current profile is divided into (N) levels. The current value of each level (In) is given by:

$$I_n = \frac{I_{\max} \cdot n}{N} \tag{6}$$

where, n is the index of the level, $n = \{1 \ldots . N\}$. in this example $N = 3$, $I_{\max}$ is the maximum value of charging or discharging currents.

- Then, all the current values are grouped into N classes and each class contains Pn elements (elements are the instantaneous values of current).

Table 3 Comparison between the real and cycling currents

Constraints	Ko40HP	
	Real cycle	Test cycle
means current, A	7.69	7.73
means charge current, A	1.28	1.29
means discharge current, A	8.79	9.03
RMS current, A	14.90	16.87
RMS charge current, A	4.69	5.33
RMS discharge current, A	14.14	16.00

$$\begin{bmatrix} I_{11} & I_{12} & \cdots & I_{1P_1} \\ I_{21} & \vdots & \vdots & \vdots \\ \vdots & \vdots & I_{ni} & I_{nP_n} \\ I_{N1} & I_{N2} & \cdots & I_{NP_N} \end{bmatrix}$$

For an individual i belongs to the class n, it is necessary that the current intensity $I(n \cdot i)$ satisfies the following condition:

$$I_{n-1} < I(n \cdot i) \leq I_n \tag{7}$$

- Finally, all the constraints generated by the current values $I(n \cdot \mathrm{Pn})$ of the level n is represented by the maximum value of current I_n during time $T(n)$ (cf. Fig. 7*b*). This is calculated so as to keep the quantity of exchanged charge ($Q(n)$) with:

$$Q(n) = \sum_{i=0}^{P_n} I(n \cdot i) \cdot \Delta T \tag{8}$$

With, ΔT the duration between two successive values of current. It therefore calculates the time $T(n)$ of a current level as follows:

$$T(n) = \sum_{i=0}^{P_n} I(n \cdot i) \cdot \frac{\Delta T}{I_n} \tag{9}$$

The classification adopted in this study allows us to move from a complex current profile to a pulse signal as offset current with well-defined current values. Furthermore and in addition to the separation of charge and discharge phases, we classified independently (see Fig. 7*a*) the constraints to urban and road parts (present in the driving cycle).

In terms of physical constraints, this classification keeps the maximum values of current consumed and recovered (see Fig. 7*b*). Table 3 compares the average and RMS values of the real current and cycling current through a single cell of the sized battery pack.

From this table, we see that the classification and the transition between the real current and the cycling current keep also the average values (the error is on the order of 1%). However, the rms cycling current is greater than real current by about 10%. The average values and rms cycling current are the physical constraints applied to the Ko40HP cells during aging tests.

The battery we want to be studied is sized for a driving range of 150 km, the cycling profiles of Fig. 7*b* obtained thanks to the classification constraints are repeated seven times to match the driving range of 150 km, and to obtain a depth of discharge (DOD) of 80%.

6 Battery modelling

In our study, the experimental results of cycling and characterisation profiles are also used to develop both the electric and aging models of Li-ion batteries. These models will be subsequently used in the future works concerning the development of energy management strategies in drivetrain applications. In this regard, the literature documents a large number of battery models with varying degrees of complexity [10]. They can be classified as electrochemical, mathematical, and equivalent electrical circuit models [11, 12]. The last category has a high potential in terms of accuracy, simplicity and the ability to predict the I–V characteristics make it suitable for dynamic modelling in power applications [13]. In our case, a dynamic model based on the non-linear equivalent circuit is proposed to describe the electric behaviours of the Li-ion battery as shown in Fig. 7*c* [14].

The battery terminal voltage obtained from the proposed model can be estimated by the following equation [14]:

$$V_{\mathrm{bat}} = V_{\mathrm{OCV}} + V_{R_\Omega} + V_{\mathrm{RC}} \tag{10}$$

© The Institution of Engineering and Technology 2017

20429746, 2017, 1, Downloaded from https://ietresearch.onlinelibrary.wiley.com/doi/10.1049/iet-est.2016.0012 by Cochrane France, Wiley Online Library on [17/04/2024]. See the Terms and Conditions (https://onlinelibrary.wiley.com/terms-and-conditions) on Wiley Online Library for rules of use; OA articles are governed by the applicable Creative Commons License

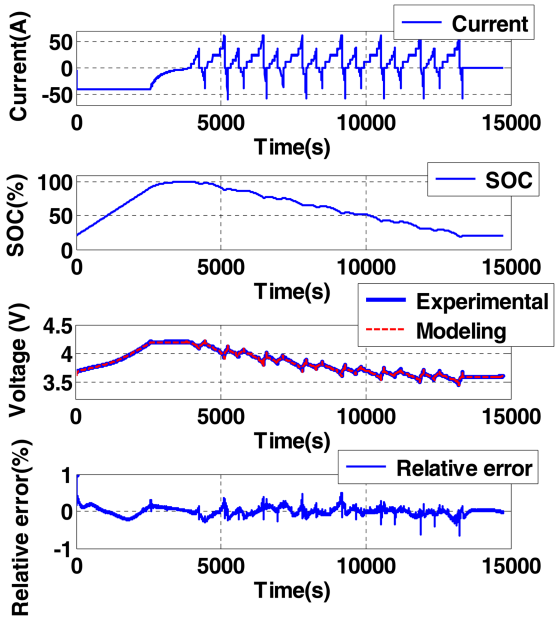

Fig. 8 *Laboratory current profile gained from a real current of ARTEMIS driving cycle*

(a) Laboratory current profile, ***(b)*** Battery SOC, ***(c)*** Experimental and modelling voltage responses, ***(d)*** Relative error

The open circuit voltage V_{OCV} according to SOC can be described as follows:

$$V_{OCV}(\text{SOC}) = x_1 + x_2 \cdot e^{(x_3 \cdot (1-\text{soc}))} + x_4 \cdot e^{(x_5 \cdot \text{soc})} + x_6 \cdot e^{(x_7 \cdot (1-\text{soc})^2)} + x_8 \cdot e^{(x_9 \cdot (\text{soc})^2)} + x_{10} \cdot e^{(x_{11} \cdot (1-\text{soc})^3)} + x_{12} \cdot e^{(x_{13} \cdot (\text{soc})^3)} \quad (11)$$

The voltage drops across battery internal resistor R_Ω related to the SOC and current sign is expressed by [14]:

$$V_{R_\Omega} = I_b \cdot \frac{x_{14}}{\sqrt{\text{soc} + x_{15} \cdot \text{soc} \cdot \text{sign}(I_b)}} \quad (12)$$

The voltage corresponds to the circuits of $R_{dll}C_{dll}$ (phenomena of double layer capacity) and $R_{dif}C_{dif}$ (diffusion proses) is given by [4]:

$$\begin{cases} V_{RC} = V_{dll} + V_{dif} \\ V_{dll}(s) = I_2(s) \cdot R_{dll} = \dfrac{1}{1 + sR_{dll}C_{dll}} \cdot \dfrac{I_b \cdot R_{dll}}{s} \\ V_{dif}(s) = I_4(s) \cdot R_{dif} = \dfrac{1}{1 + sR_{dif}C_{dif}} \cdot \dfrac{I_b \cdot R_{dif}}{s} \\ I_1 + I_2 = I_3 + I_4 = I_b \end{cases} \quad (13)$$

where the time constants for $R_{dll}C_{dll}$ and $R_{dif}C_{dif}$ circuits are $\tau_{dll} = R_{dll}C_{dll}$ and $\tau_{dif} = R_{dif}C_{dif}$, respectively. The parameters $x_{1\ldots15}$ represent the fitting parameters of the Li-ion battery model.

Fig. 8*a* illustrates the laboratory current profile gained from a real current of ARTEMIS driving cycle. This profile used for aging cycling tests represents seven ARTEMIS driving cycle with a 150 Km of driving range. The tested battery is first charged thanks to constant-current/constant-voltage (CC/CV) charge protocol.

The battery stat of charge (SOC) is the ratio between residual capacity and actual maximum capacity:

$$\text{SOC}(t_1) = 100 * \frac{Q_{bat_{res}}}{Q_{bat_{act}}} = \text{SOC}(t_0) - \frac{100}{C_{bat\_act}} \int_{t_0}^{t_1} i_{bat}(t)\, dt \quad (13b)$$

Avec: SOC (t_0) is the initial stat of charge and $i_{bat}(t)$ is the battery current; Q_{bat_res}: residual capacity (Ah) à $t = t_1$; C_{bat_act}: actual maximum capacity (Ah).

The SOC evolution during the cycling test is shown in Fig. 8*b*, which is varied from 100% to lower value so at 25% with 80% of DOD. Fig. 8*c* shows the comparison between the experimental voltage response and battery model. It can also be seen that the battery model matches very well the electrical behaviour of the Li-ion battery over a wide range of operating points. Fig. 8*d* illustrates the relative error between the modelling and experimental responses during a full mission of EV. It can be observed that the relative error stays below 1% for a wide range of SOC variation (100 to 20%). This result proves the high accuracy and the best performance of the proposed model based on the non-linear equivalent circuit in drivetrain applications.

7 Thermal behaviour during cycling

In this section, we present the thermal response of the Ko40HP cells during cycling. The cells were placed in a climatic chamber at 23°C to meet the temperature conditions specified by the manufacturer. Temperature measurements are given by three sensors placed on the cell surface. During the cycling phase, the maximum current of the cells is about 52 A, which represents 1.3 C of rate current.

According to the temperature measurements, we can distinguish the charging and cycling phases (see Fig. 9*a*).

The temperature of the Ko40HP cells is higher in the charging phase. In this phase, specifically, during the constant current charging (CC), the temperature increases from 23.5 to 26.1°C. During cycling phase, the cells temperature is lower and varies between 23.7 and 24.6°C. Regarding the measurement error, it is found that the values given by the three sensors are substantially equal.

8 Aging using 1C/1C cycles

The manufacturer of the tested cells Kokam Ko40HP gives some aging results at an ambient temperature around 23°C with 1 C of charging current (CC-CV) until 4.2 V and a discharge current of 1 C to 3 V. According to the measurements obtained and shown in Fig. 9*b*, the cells lose 20% of their capacity after 1600 cycles. At the beginning of cycling, the loss of capacity is relatively small; it is around 5% for the first 800 cycles. Thereafter, the degradation is accelerated and decrease linearly according to the number of cycles performed.

9 Aging during real use of the battery

The battery aging is evaluated by measurements of internal resistance and capacity [15]. These characteristics are computed using currents and voltages data. The characterisation cycles have been defined based on international standards, such as IEC 62660-1/2. This standard requires a complete recharging of the battery cell followed by a constant current discharge to the final voltage given by the manufacturer (Fig. 9*c*).

9.1 Capacity degradation

To compute the capacity, we measure the energy that the battery cell can store during a recharging phase or it can provide during a discharge phase [16]. We chose to estimate it for a 40 A discharge current (1 C). Energy (E^i_{dech}) discharged by the battery cell at the instant (i) cycling is given by:

$$E^i_{dech} = \int_0^{t_D} V \cdot I \cdot dt \quad (14)$$

where I and V represent, respectively, the discharge current and the instantaneous voltage of the battery cell. t_D is the duration of the discharge phase (see Fig. 9*c*). This duration decreases with time because of the cells aging.

© The Institution of Engineering and Technology 2017

20429746, 2017, 1, Downloaded from https://ietresearch.onlinelibrary.wiley.com/doi/10.1049/iet-est.2016.0012 by Cochrane France, Wiley Online Library on [17/04/2024]. See the Terms and Conditions (https://onlinelibrary.wiley.com/terms-and-conditions) on Wiley Online Library for rules of use; OA articles are governed by the applicable Creative Commons License

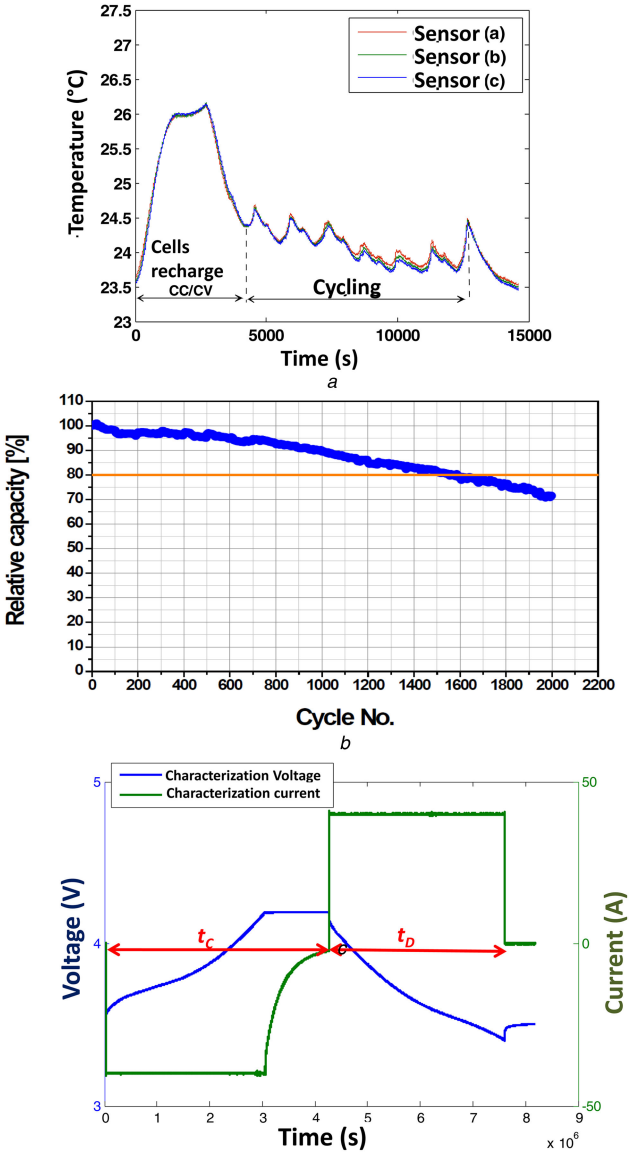

Fig. 9 *Thermal response during aging cycle and characterisation cycle*
(a) Temperature of the Ko40HP cell (three sensors a. b and c) during the cycling, ***(b)*** Ageing of the 40 Ah HP Kokam cell at 1 C/1 C current [4], ***(c)*** current and voltage of the battery cell during the characterisation charge/discharge cycle. Discharge at 1c (40 A) and CC/CV charge (Constant Current/ Constant Voltage)

The capacity decreasing due to the cells aging is estimated according to the energy (E^0_{dech}) at the start of the cycling test. The variation of the capacity (ΔC^i) at time (i) with respect to the energy discharged at this time is expressed by:

$$\Delta C^i(\%) = \left(1 - \frac{E^i_{\text{dech}}}{E^0_{\text{dech}}}\right) \cdot 100 \tag{15}$$

To estimate the useful life of tested battery, we evaluate the variation of capacity and internal resistance during cycling test. This measurement data allows us to identify the parameters values of the battery aging model. However, this tool could be used to test the manufacturer warranty, and thus the impact of driving cycles and energy management strategies on battery lifetime. In this context, a Li-ion battery aging model based on semi-empirical approach is selected to describe the electrochemical degradation processes. The chosen model is represented by the following equation involving three parts relate to time, temperature and operating voltage [15]:

$$a_{\text{bat}}(t, V, T) = a_{\text{init}} \cdot [1 + c_a \cdot \sqrt{t}(c_{\text{T}}^{(T - T_0)/\Delta T} \cdot c_V^{(V - V_0)/\Delta V}] \tag{16}$$

where a_{init} represents the initial lifetime of battery. The parameters V and T are the average voltage and temperature of the battery cell, respectively. The related reference parameters T_0, V_0, ΔT and ΔV can be chosen according to battery technology and test conditions. However, c_a, c_{T} and c_V are the fitting parameters for capacity fade and resistance increase.

It must be noted that the traction battery is usually considered at the end-of-life when the battery capacity is decreased by 20% of its initial value. As a result, the results below are obtained after about 3200 cycles of charge/discharge by using the laboratory current profile gained from a real current of ARTEMIS driving cycle.

Fig. 10*a* represents the comparison of the simulation with the experimental data of capacity fade for verification of the proposed model. The capacity estimation is carried out thanks to the ratio (in %) between the current and initial capacity of the tested battery. At the beginning, we can observe the stabilisation of the capacity evolution and after about 700 cycles of charge/discharge, the decreasing of the capacity start and continuous the decreasing linearly according to the number of cycles fulfilled. The degradation it is about 1%/100 cycles and reach the 20% at 3150 cycles, what correspond to 472,500 km when we use the vehicle in a continuous manner. These results prove the good lifetime of this technology under real conditions of use. On the other hand, it can be clearly seen that there is no global divergence and no great mismatch between the modelling and experimental aging responses. The close agreement between modelling results and experimental data indicates that the aging model of tested battery can make a reliable lifetime predictions concerning capacity fade. This is also confirmed by the low relative error is shown in Fig. 10*a*, which the total error band is less than 2%.

9.2 Inner resistance degradation

To estimate the internal resistance, we operate the charging and discharge characterisation cycle. At the end of cycle (i), the energy stored in the battery is noted E^i_{bat}. If we assume that all of the losses during charging and discharging are related to the internal resistance and that resistance has the same value for the charge and discharge. We can write the energy E^i_{bat} using the expression below:

$$\begin{cases} E^i_{\text{bat}} = E^i_{\text{dech}} + R^i \displaystyle\int_0^{t_D} I^2 \cdot \mathrm{d}t \\ E^i_{\text{bat}} = E^i_{\text{cha}} - R^i \displaystyle\int_0^{t_C} I^2 \cdot \mathrm{d}t \end{cases} \tag{17}$$

where, E^i_{cha} is the stored energy during the charging phase during the time t_C (see Fig. 9*c*). It is expressed by:

$$E^i_{\text{cha}} = \int_0^{t_C} V \cdot I \cdot \mathrm{d}t \tag{18}$$

The internal resistance (R^i) of a battery cell at the instant (i) is calculated by:

$$R^i = \frac{E^i_{\text{cha}} - E^i_{\text{dech}}}{\int_0^{t_D} I^2 \cdot \mathrm{d}t + \int_0^{t_C} I^2 \cdot \mathrm{d}t} \tag{19}$$

In the same way as the capacity, the variation of the internal resistance (ΔR^i) is given, according to initial value of internal resistance (R^0), by:

$$\Delta R^i(\%) = \left(1 - \frac{R^i}{R^0}\right) \cdot 100 \tag{20}$$

The internal resistance is another parameter, which changes during the cycling of battery cells [17]. Fig. 10*b* presents the comparison

© The Institution of Engineering and Technology 2017

20429746, 2017, 1, Downloaded from https://ietresearch.onlinelibrary.wiley.com/doi/10.1049/iet-est.2016.0012 by Cochrane France, Wiley Online Library on [17/04/2024]. See the Terms and Conditions (https://onlinelibrary.wiley.com/terms-and-conditions) on Wiley Online Library for rules of use; OA articles are governed by the applicable Creative Commons License

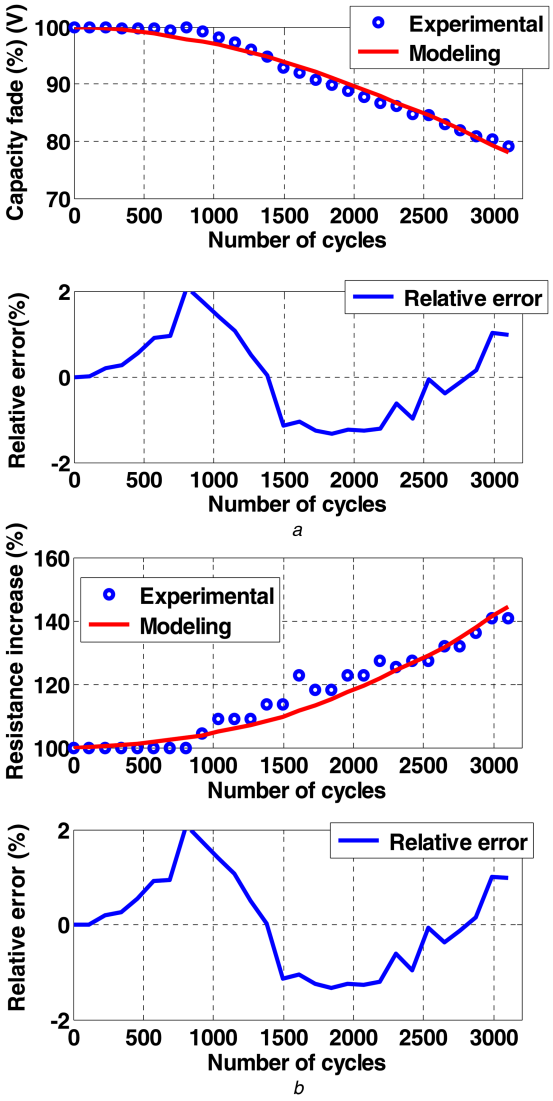

Fig. 10 *Experimental and modelling of Li-ion battery aging*
(a) Experimental and modelling responses of Li-ion battery capacity fade and Relative error, ***(b)*** Experimental and modelling responses of Li-ion battery resistance increase and Relative error

between measured and simulated internal resistant during cycling test.). First, it is found that the internal resistance of the tested battery does not reach the maximum value of degradation at the end-of-life estimates normally about 100% or so above initial value. After 3200 cycles of charge/discharge, the aging does not exceed 42%. On the other hand, the proposed aging model shows a good agreement with the experimental response of the internal resistant over the cycling test. The relative error between the simulated and the measured internal resistant is shown in Fig. 10*b*. It can be observed that the maximal of the relative error stays below 2% during the entire test of aging cycling.

10 Conclusion

This paper deals with the study of a HP Li-ion technology behaviour in real conditions of use. After the sizing of embedded source with different driving range and using several technologies, we have shown the benefit of the power Li-ion technology in lower and medium ranges (less than 250 km). Before beginning the experimental study, we presented the test bench developed in our laboratory, which is used to characterise the storage components. In the second part of the paper, we achieved a simplification study of the recorded ARTIMIS cycle. These cycles were used for the modelling of the electrical, thermal and aging behaviours of KOKAM 40Ah HP cells. The results have shown this interesting type of component with a possibility of using this component during 472,500 km with continuous use for nearly 3 years.

11 References

[1] Graham, L., Christenson, M., Karman, D.: 'Light duty hybrid vehicles-influence of driving cycle and operating temperature on fuel economy and GHG emissions'. IEEE, 2006

[2] André, M.: 'Real-world driving cycles for measuring cars pollutant emissions - Part A: The ARTEMIS European driving cycles'. Report INREST-LTE 0411, June 2004

[3] http://www.bluecar.fr, consulté le: 09-12-2012

[4] http://www.saftbatteries.com/

[5] Sadoun, R., Rizoug, N., Bartholomeüs, P., *et al.*: 'Influence des cycles de conduite sur le dimensionnement du système de stockage hybride batterie-Supercondensateur alimentant un véhicule électrique'. EF'11, Belfort, Décembre 2011

[6] http://www.dowkokam.com/

[7] Sadoun, R., Rizoug, N., Bartholomeus, P., *et al.*: 'Influence of the drive cycles on the sizing of hybrid storage system Battery-Supercapacitor supplying an electric vehicle'. 37th Annual Conf. on IEEE Industrial Electronics Society, IECON11, Melbourne, 2011, pp. 4106–4112

[8] Sadoun, R., Rizoug, N., Bartholomeus, P., *et al.*: 'Sizing of hybrid supply (Battery-Supercapacitor) for electric vehicle taking into account the weight of the additional buck-boost chopper'. IEEE-Conf. REVET12, Hammamet, February 2012

[9] Rizoug, N.: 'Modélisation électrique et énergétique des supercondensateurs et méthodes de caractérisation: application au cyclage d'un module de supercondensateur basse tension en grande puissance'. *Thèse de doctorat*, École Centrale de Lille, 2006

[10] Mesbahi, T., Rizoug, N., Bartholomeus, P., *et al.*: 'Li-ion battery emulator for electric vehicle applications'. 2013 IEEE Vehicle Power and Propulsion Conf. (VPPC), 2013, pp. 1–8

[11] Bhide, S., Shim, T.: 'Novel predictive electric Li-ion battery model incorporating thermal and rate factor effects', *IEEE Trans. Veh. Technol.*, 2011, **60**, (3), pp. 819–829

[12] Chen, M., Rincon-Mora, G.A.: 'Accurate electrical battery model capable of predicting runtime and I–V performance', *IEEE Trans. Energy Convers.*, 2006, **21**, (2), pp. 504–511

[13] Zhang, L., Wang, L., Hinds, G., *et al.*: 'Multi-objective optimization of lithium-ion battery model using genetic algorithm approach', *J. Power Sources*, 2014, **270**, pp. 367–378

[14] Mesbahi, T., Khenfri, F., Rizoug, N., *et al.*: 'Dynamical modeling of Li-ion batteries for electric vehicle applications based on hybrid Particle Swarm–Nelder–Mead (PSO–NM) optimization algorithm', *Electr. Power Syst. Res.*, 2016, **131**, pp. 195–204

[15] Ecker, M., Gerschler, J.B., Vogel, J., *et al.*: 'Development of a lifetime prediction model for lithium-ion batteries based on extended accelerated aging test data', *J. Power Sources*, 2012, **215**, pp. 248–257

[16] Urbain, M.: 'Modélisation électrique et énergétique des accumulateurs Lithium-ion en ligne du SOC et de SOH'. *Thèse de doctorat*, Institut National Polytechnique de Lorraine, 2009

[17] Nadeau, J., Dubois, M.R., Desrochers, A., *et al.*: 'Ageing estimation of Lithium-ion batteries applied to a three-wheel PHEV roadster'. 2013 IEEE Vehicle Power and Propulsion Conf. (VPPC), Beijing, 2013, pp. 1–6

© The Institution of Engineering and Technology 2017

20429746, 2017, 1, Downloaded from https://ietresearch.onlinelibrary.wiley.com/doi/10.1049/iet-est.2016.0012 by Cochrane France, Wiley Online Library on [17/04/2024]. See the Terms and Conditions (https://onlinelibrary.wiley.com/terms-and-conditions) on Wiley Online Library for rules of use; OA articles are governed by the applicable Creative Commons License